Materials Letters 196 (2017) 64–68

Contents lists available at ScienceDirect

Materials Letters

journal homepage: www.elsevier.com/locate/mlblue

Nanoscale investigation of ferroelectric and piezoelectric properties in (Pb,Ca)TiO_3 thin films grown on $LaNiO_3$/$LaAlO_3$(100) and Pt/Si(111) using piezoresponse force microscopy

R.A. Capeli [a], F.M. Pontes [a,*], D.S.L. Pontes [b], A.J. Chiquito [c], W.B. Bastos [f], Marcelo A. Pereira-da-Silva [d,e], E. Longo [b,f]

[a] Department of Chemistry, Universidade Estadual Paulista – Unesp, P.O. Box 473, 17033-360 Bauru, São Paulo, Brazil
[b] LIEC – Department of Chemistry, Universidade Federal de São Carlos, Via Washington Luiz, Km 235, P.O. Box 676, 13565-905 São Carlos, São Paulo, Brazil
[c] NanO LaB – Department of Physics, Universidade Federal de São Carlos, Via Washington Luiz, Km 235, P.O. Box 676, 13565-905 São Carlos, São Paulo, Brazil
[d] Institute of Physics of São Carlos, USP, São Carlos 13560-250, São Paulo, Brazil
[e] UNICEP, São Carlos 13563-470, São Paulo, Brazil
[f] Institute of Chemistry, Universidade Estadual Paulista – Unesp, Araraquara, São Paulo, Brazil

ARTICLE INFO

Article history:
Received 23 January 2017
Received in revised form 1 March 2017
Accepted 4 March 2017
Available online 6 March 2017

Keywords:
Thin films
PFM
Buffer layer
Epitaxial growth

ABSTRACT

Single phase polycrystalline and strong textured $Pb_{0.76}Ca_{0.24}TiO_3$ (PCT24) thin films have been grown on platinum coated silicon and $LaAlO_3$(100) (LAO) substrates using $LaNiO_3$ (LNO) as a buffer layer by chemical solution deposition. X-ray diffraction measurements showed that the PCT24 thin films crystallize in a highly *a*-oriented single phase on LNO/LAO(100). The effects of the LNO buffer layer, nature of the substrate, and film orientation on the ferroelectric and piezoelectric properties were investigated in the nanoscale range using piezoresponse force microscopy (PFM). Local piezoelectric hysteresis loops for PCT24/LNO/LAO(100) oriented films and PCT24/Pt/Si polycrystalline films were measured on selected grains. From these piezoloops, PCT24/LNO/LAO(100) oriented films show a higher response (maximum relative d_{33} value) than PCT24/Pt/Si polycrystalline films. Furthermore, the comparison of simultaneously acquired surface morphology and piezoresponse images of the PCT24/Pt/Si films revealed the presence of inactive grain regions. In contrast, highly *a*-oriented films showed a higher presence of active grains. Our observations suggest that the improvement of ferro/piezoelectric properties is greatly associated with the use of LNO buffer layers and the growth of highly *a*-oriented films.

1. Introduction

Perovskite ABO_3 oxide thin films are recognized as promising materials for the development of numerous applications such nanocrystalline ferroelectric memories, sensors, ferroelectric-gate thin film transistors, catalysis, optical devices, and photovoltaic cell [1–5]. A variety of approaches such as compositional engineering (*CEng*), epitaxial heterostructure growth engineering (*EHGEng*), and buffer layer engineering (*BLEng*) have been utilized to tailor the properties of perovskite ABO_3 oxide thin films [6–11]. Usually a buffer layer is required to facilitate nucleation, preventing unwanted reactions at the film/substrate interface and in some cases also it acts as a base electrode.

For use as a buffer layer, $LaNiO_3$ (LNO) perovskite is perhaps the most researched and technologically important compound proposed as an alternative to conductive oxide electrodes [12–14]. Using (100) Si substrates and $LaNiO_3$ buffer layers Song et al. have fabricated a-axis oriented $Bi_{0.25}Nd_{0.85}Ti_3O_{12}$ (BNT) thin films on $LaNiO_3$/Si(100) using pulsed laser deposition [15]. The good electrical properties exhibited by the films suggest great future for BNT/LNO/Si(100) structures as ferroelectric gate transistors (FGTs). Concerning the *EHGEng* approach, Langenberg et al. have reported the epitaxial growth of $(Sr_{1-x}Ba_x)MnO_3$ thin films by pulsed laser deposition onto (001)-oriented perovskite substrates [16]. The authors showed that thin film growth is completely strained by the emergence of new phases. Recently, Tang et al. reported the growth of $Bi_{3.15}Nd_{0.85}Ti_3O_{12}$-$La_{0.7}Ca_{0.3}MnO_3$ composite thin films on $LaNiO_3$ buffered $SrTiO_3$ crystal substrates by radio frequency (rf) magnetron sputtering [17].

* Corresponding author.
E-mail address: fenelon@fc.unesp.br (F.M. Pontes).

http://dx.doi.org/10.1016/j.matlet.2017.03.029
0167-577X/

It is therefore imperative to investigate the factors (e.g., substrate selection, buffer layer material choice, and chemical composition) that govern the composition-structure-property relationship. In this regard, scanning probe microscopy (SPM) technique is a powerful tool for the investigation of a wide range of properties (optical, conductive, magnetic, crystallographic, chemical, biological, microstructural, dielectric, piezoelectric, and ferroelectric) at the nanoscale range [18–20]. Recently, Huo et al. reported a large piezoelectric response for Li^{+}-Nb^{5+} pair doped-$BiFeO_3$ polycrystalline thin films using piezoresponse force microscopy [21]. Fu et al. studied the variation of local piezoelectricity in $CoFe_2O_4$-$Pb(Zr_{0.3},Ti_{0.7})$ nanofibers using piezoresponse force microscopy [22]. In addition, Xiao studied the effect of LNO and platinum electrodes on the piezoelectric performance of $BiScO_3$-$PbTiO_3$ (BSPT) thin films by piezoelectric force microscopy [23].

In this work, advanced characterization tools such as atomic force microscopy (AFM) and piezoresponse force microscopy (PFM) were employed to investigate the local microstructural and piezo/ferroelectric properties of the PCT24 thin films grown on $LaNiO_3$/LaAlO(100) and platinum coated silicon substrates.

2. Experimental procedure

$Pb_{0.76}Ca_{0.24}TiO_3$ (PCT24) thin films and $LaNiO_3$ (LNO) buffer layers used in this study were produced by chemical solution deposition. Details of the preparation method can be found in literature [24,25].

LNO buffer layers were grown on commercially available (100) $LaAlO_3$ substrates before deposition of PCT24 thin films using a spin coater (KW-4B, Chemat Technology) operating at 7200 revolutions/min for 30 s. Each layer was annealed using a hot plate preheated to 150 °C for 5 min for drying followed by pre-firing in a tube furnace at 400 °C for 4 h at a heating rate of 5 °C/min in an oxygen atmosphere to pyrolyze the organic materials. This was subsequently followed by heating at 700 °C for 2 h at a heating rate of 5 °C/min under an oxygen atmosphere for crystallization. The film thickness was controlled by adjusting the number of coatings and the rotation. Each layer was pyrolyzed at 400 °C and crystallized at 700 °C before deposition of the next layer. The coating/drying operations were repeated until the desired thickness was obtained.

Lastly the deposition of PCT24 thin films on the LNO/LAO(100) heterostructure and platinum coated silicon substrates was carried out using a spin coater (KW-4B, Chemat Technology) also operating at 7200 revolutions/min for 30 s. In this case, the PCT24 thin films were annealed at 400 °C for 4 h and then at 650 °C for 2 h in a tube furnace under an oxygen atmosphere. In this process, the desired thickness was obtained by repeating the spin-coating and heat treatment cycles.

The crystal structures of PCT24/LNO/LAO(100) and PCT24/Pt/Si samples were investigated by X-ray diffraction (XRD) using a Rigaku D/Max-2400 diffractometer. The thicknesses of the PCT24 thin films and LNO buffer layers were evaluated using FEG-SEM (FEG-VP Zeiss Supra 35) with a secondary electron detector to observe freshly fractured film/substrate cross-sections. The surface microstructures of these samples were characterized using atomic force microscope (AFM). A Bruker Dimension ICON was used for these experiments.

The domain structures and local piezohysteresis loops of PCT24 thin films were investigated in the nanoscale level using a commercial atomic force microscope (AFM) (MultiMode Nanoscope V, Bruker) modified to perform piezoresponse force microscopy (PFM). The system was equipped with a lock-in amplifier (SR850, Stanford) and a function generator (33220A, Agilent). During the PFM measurements, the conductive probe was electrically grounded and an external voltage was applied to the LNO buffer layer (serving as a bottom electrode). The platinum electrode was operated with a driving amplitude of 1 V (RMS).

3. Results and discussions

Fig. 1(a)–(c) presents the θ-2θ X-ray diffraction patterns of the $LaAlO_3$(100) crystal substrate, PCT24/LNO/LAO(100), and PCT24/Pt/Si samples, respectively. It can be observed from Fig. 1 (b) and (c) that all of the thin films are well crystallized and contain a single perovskite phase. Furthermore, only (l00) reflections of the PCT24 and LNO thin films and the corresponding peaks of the LAO substrates (marked "#") were clearly observed for all thin films, except for a small portion of (00l) reflections which can be found in the PCT24 thin films. This suggests that all the thin films are highly (100)-oriented [Fig. 1(b)]. In contrast, all the thin films grown on platinum coated Si(111) substrates display a polycrystalline nature [Fig. 1(c)]. The LNO buffer layer and ferroelectric PCT thin films have pseudocubic and tetragonal structures respectively. For the PCT24 thin films, the lattice parameters for tetragonal symmetry calculated from the measured in-plane (a) and out-of-plane (c) were found to be 0.389 nm and 0.391 nm for films grown on LNO/LAO and 0.399 and 0.403 nm for films grown on Pt/Si, respectively.

The inset of Fig. 1 shows the surface morphologies of the thin films obtained using atomic force microscopy. As shown in Fig. 1 (d–f), the surface morphology of all films displays nanometer grain sizes. A crack/pinhole free, dense and smooth surface morphology has been obtained for the LNO buffer layer grown on LAO(100), as seen in Fig. 1(d). The root mean square (R_{ms}) roughness for scan areas of $2 \times 2\ \mu m^2$ was 4.2 nm with average grain size of 25 nm for LNO thin films grown on LAO(100). For the PCT24 thin films grown on LNO/LAO(100) [Fig. 1(e)] and platinum coated silicon substrate [Fig. 1(f)] the surface morphology was homogenous, with a granular-like surface. The average grain size was found to be ~50 nm for PCT24 thin films grown on LNO/LAO(100) and 130 nm for PCT24 thin films grown on platinum coated silicon. The root mean square (R_{ms}) values of roughness for scan areas of $2 \times 2\ \mu m^2$ were 10.0 nm and 4.5 nm for PCT thin films grown on platinum coated Si and LNO/LAO(100), respectively. In addition, thicknesses of 150 nm, 200 nm, and 220 nm were obtained for LNO on LAO(100), PCT24 on LNO/LAO(100) and PCT24 on platinum coated silicon substrate, respectively.

The observed differences in the thin films surface morphologies, roughness, grain size, and orientation play a key role in determining the ferroelectric behavior of nano and macroscale devices.

Fig. 2(a–d) show piezoelectric images of PCT24 thin films, acquired simultaneously with the topography scans. All images were taken under identical acquisition conditions. The same probe, AC signal applied, and frequency were used for each image.

The out-of-plane PFM images show that the domain structures appear as bright, dark and intermediate grey regions distributed throughout the surface of the thin films [26,27]. The out-of-plane PFM image for the PCT24/LNO/LAO(100)-oriented sample shows a piezoactivity signal on the whole surface [Fig. 2(d)], confirming the good quality of the films. This result can be interpreted as follows: the LNO-epitaxial buffer layer allowed a homogenous nucleation, followed by the growth of the perovskite films and finally, giving rise to a homogenous piezoactivity signal. Unfortunately, the PCT/Pt/Si polycrystalline sample [Fig. 2(b)] exhibits some regions with no piezoactivity (blue arrow), i.e., some grains seem to behave as if they do not have out-of-plane and in-plane polarization components.

The local comparison between the topography and out-of-plane PFM images unambiguously allows a correlation between the grain

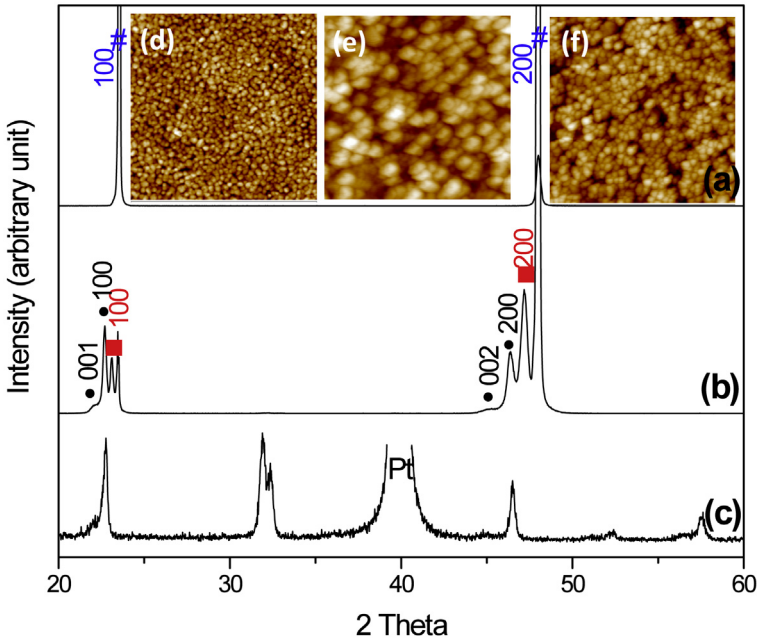

Fig. 1. X-ray diffraction patterns of (a) the $LaAlO_3$(100) crystal substrate, (b) PCT24/LNO/LAO(100) films and (c) PCT24/Pt/Si films. AFM images of (d) $LaNiO_3$(LNO) films grown on $LaAlO_3$(100) crystal substrate, (e) PCT24 films grown on platinum coated silicon substrate and (f) PCT24 films grown on LNO/LAO(100). PCT24 thin films (●), LNO thin films (■) and LAO(100) crystal substrate (#). AFM images (scan size = 2 μm).

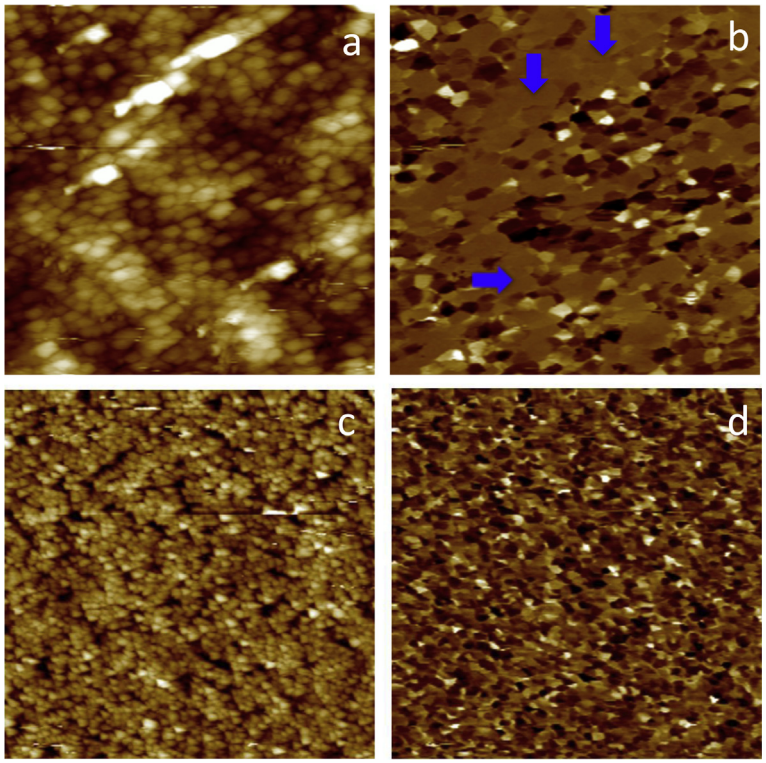

Fig. 2. Surface topography (left) and out-of-plane PFM images (right) of PCT24 films (a–b) grown on platinum coated silicon substrates and (c–d) grown on LNO buffer layers on LAO(100) crystal substrates. Blue arrows indicate zero piezosignal region. Scan size = 5 μm. (For interpretation of the references to colour in this figure legend, the reader is referred to the web version of this article.)

size and domain structure. From this comparative analysis, it can be concluded that most of the domain structure is limited by the grain size of film, i.e., the domain wall motion is limited by the grain boundaries.

In order to investigate localized polarization switching behaviors for PCT24 thin films, a DC bias was applied to the conducting PFM-tip probe while scanning the desired area. Local poling "writing" was achieved on a square-shaped region (2 μm × 2 μm,

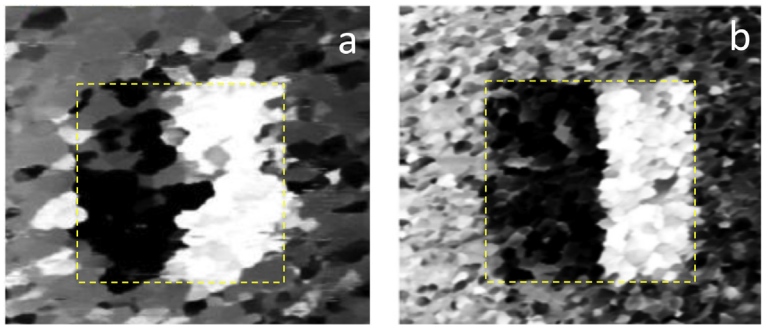

Fig. 3. Characteristic out-of-plane PFM images of (a) PCT24 films grown on platinum coated silicon substrates and (b) PCT24 films grown on LNO buffer layers on LAO(100) crystal substrates after poling with +15 V (bright contrast) and −15 V (dark contrast). Scan size = 4 μm.

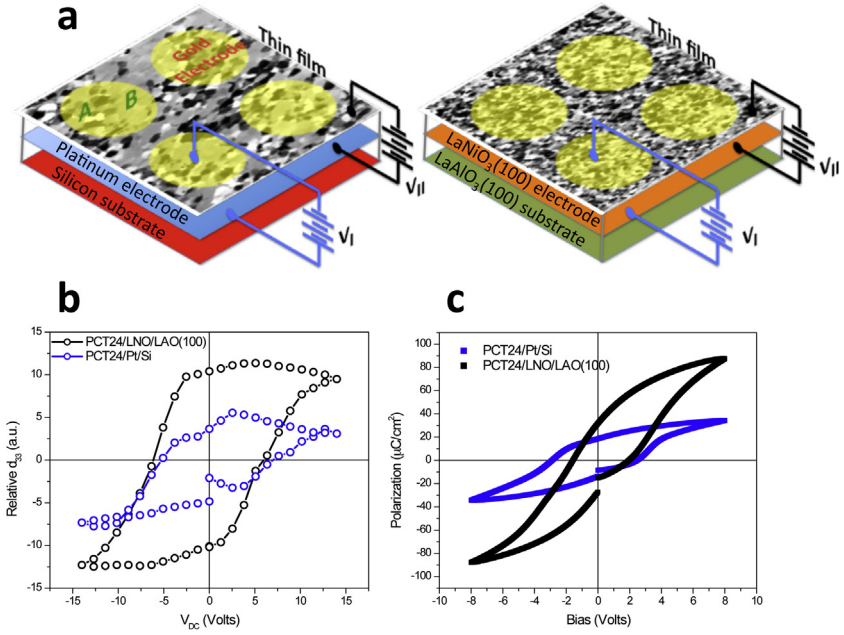

Fig. 4. (a) Schematic diagram of the Au/PCT24/Pt/Si and Au/PCT24/LNO/LAO(100) structures: V_I is the polarization voltage applied between the Pt and Au electrode in order to measure macroscopic hysteresis while V_{II} is the polarization voltage applied between the PFM conductive tip in contact mode and LNO electrode in order to measure local piezohysteresis. A and B denote areas with and without piezosignal response, respectively. The yellow circle represents an Au electrode with a diameter of 200 μm. (b) Local piezohysteresis loops (on individual grains) of PCT24/LNO/LAO(100) and PCT24/Pt/Si films. (c) Macroscopic hysteresis loops of PCT24/LNO/LAO(100) and PCT24/Pt/Si films. (For interpretation of the references to colour in this figure legend, the reader is referred to the web version of this article.)

dashed yellow line) by applying an alternating DC voltage of −15 V (black contrast) and +15 V (bright contrast) to the conductive PFM-tip, corresponding to downward and upward polarization stable states respectively. This approach is illustrated in Fig. 3. After applying an alternating DC voltage, strong domain patterns are clearly visible on the PFM images, as shown in Fig. 3(a) and (b). This indicates that the local polarization can be switched. In the case of the PCT24/Pt/Si sample the PFM image clearly shows some unchanged regions after applying +15 and −15 V to the tip (a dashed line indicates the area which was subjected to the electric field). This might be due to the presence of some piezoelectric inactive grains inside the film and/or domain-wall pinning, as depicted in Fig. 3(a). On the other hand, it should be noted that in the case of the PCT24/LNO/LAO(100) oriented film, the region surrounded by the yellow dashed line revealed an almost uniform contrast (dark and bright regions), shown in Fig. 3(b). This observation should be interpreted as follows: the inclusion of a highly oriented conducting LNO buffer layer improves the quality of the thin film (PCT24) and leads to an improved homogeneity of domain switching.

To acquire more detailed information on ferroelectric polarization switching, local piezoelectric hysteresis loops were measured by positioning the probing PFM-tip at a chosen individual grain on the film surface and recording the piezosignal as a function of an applied DC voltage. In addition, macroscopic hysteresis loops were recorded for comparison. The schematic diagram and measurement results are shown in Fig. 4(a–c). Fig. 4(a) shows a schematic diagram of the structures Au/PCT24/Pt/Si and Au/PCT24/LNO/LAO (100). Fig. 4(b) shows typical piezohysteresis loops for both oriented and polycrystalline films. The presence of these hysteresis loops confirms the presence of locally switchable polarization. It can be noted that the PCT24/LNO/LAO(100) oriented films show defined and well-saturated piezohysteresis loops with a maximum relative d_{33} (arbitrary unit) value much higher than that of PCT24/Pt/Si polycrystalline films (experiments were performed with same type of cantilevers). This clearly suggests an enhancement of the ferroelectric properties, commonly attributed to the high orientation quality of the PCT24/LNO/LAO(100) films. A Radiant Precision Premier II system was employed to measure the macroscopic hysteresis loops for the Au/PCT24/Pt/Si and Au/PCT24/LNO/LAO(100)

structures, as shown in Fig. 4(c). We note that the macroscopic polarization switching results are similar to previous local piezo-hysteresis loops. However, it should be noted that the macroscopic hysteresis loops for the Au/PCT24/Pt/Si structure correspond to grain regions with and without piezoactivity. On the other hand, there are several reports in the literature where the piezoelectric and ferroelectric properties show a dependence on the thickness of thin films [28,29]. The macroscopic properties may change as a function of the thickness of each sample analyzed. In these measurements, the capacitor model, i.e. Conductor-Ferroelectric-Con ductor, is generally used. Thus, the results obtained from polarization measurements (curve P vs. E) are directly dependent on the electric field which, in turn, depends on the thickness of the material. This electric field is assumed parallel and uniform along the thickness of the sample, obviously neglecting edge effects, (in the thin film this effect is very small). This thickness controls to the intensity of the electric field (E = V/d) that the sample is subjected to. In addition, the macroscopic properties correspond to the total response of tens of grains of the thin film contained between the electrodes in the "capacitor model". In other words, they are a result of thousands of local responses from each grain of the thin film.

In the nanoscopic regime, where the response obtained from the tip of the PFM (tip) is local, we have two effects to consider: i) The electric field is extremely intense under the energized probe. This electric field decreases in intensity along the thickness of the sample. From mathematical modeling we found a radial dependence of the electric field obeying a r^2 law. Thus, d33 tensor element is obtained from the specific grain where the probe is positioned and effectively the field acts on the first ~50 nm of the thickness just below the probe. ii) Each grain does respond with different intensities because the thin film is polycrystalline and the direction of spontaneous polarization is different in each grain. In some grains it may even be null.

4. Conclusions

In summary, PCT24/LNO/LAO(100) oriented and PCT24/Pt/Si polycrystalline thin films have been successfully fabricated by a chemical solution deposition method. The local piezoelectric response for PCT24/LNO/LAO(100) oriented and PCT24/Pt/Si polycrystalline films was investigated using piezoresponse force microscopy. Results of the ferroelectric domain structure investigation, domain switching behavior and piezoelectric hysteresis loops with nanometer resolution combined with structural investigations by XRD, provided clear evidence of the effects of the LNO (100) oriented buffer layer and the substrate nature on the piezoelectric properties of the PCT24 films. The results suggest that LNO (100) highly a-oriented buffer layers (electrode) significantly enhanced the ferroelectric properties, also improving the domain structure growth quality. For the PCT24/Pt/Si polycrystalline films, some inactive grain regions (piezosignal zero) were observed. This may be attributed to poor film/substrate interface quality and/or grains with crystallographic orientation; for example, no out-of-plane and in-plane spontaneous polarization components were observed.

Therefore, from a technological viewpoint our results suggest that is vital to get the maximum information relating to the piezoelectric/ferroelectric properties at the nanoscale for better understanding of the apparent contradiction in macroscopic measurements.

Acknowledgments

This study was financially supported by the Brazilian agencies FAPESP and CNPq. We would like to thank CEPID/CMDMC/INCTMN/CDMF, FAPESP (processes n°. 11/20536-7, 12/14106-2, and 13/07296-2) and CNPq (process n°. 470147/2012-1).

References

[1] R. Nechache, W. Huang, S. Li, F. Rosei, Nanoscale 8 (2016) 3237–3243.
[2] Z. Huiyuan, Z. Pengfei, D. Sheng, ACS Catal. 5 (2015) 6370–6385.
[3] P. Debashis, Y.T. Tseung, Ferroelectrics 471 (2014) 23–64.
[4] T. Tomohisa, T. Satoko, S. Youichi, J. Sens. Technol. 2 (2012) 75–81.
[5] G. Ilya, D.V. West, T. Maria, G. Gaoyang, M.S. David, W. Liyan, C. Guannan, M.G. Eric, R.A. Andrew, K.D. Peter, E.S. Jonathan, M.R. Andrew, Nature 503 (2013) 509–512.
[6] N. Ortega, K. Ashok, R. Oscar, O.A. Maslova, I.Y. Yu, J.F. Scott, R.S. Katiyar, J. Appl. Phys. 114 (2013) 104102–104109.
[7] S. Fernandez-Peña, C. Lichtensteiger, P. Zubko, C. Weymann, S. Gariglio, J.M. Triscone, APL Mater. 8 (2016) 086105–086108.
[8] J.C. Agar, A.R. Damodaran, M.B. Okatan, J. Kacher, C. Gammer, R.K. Vasudevan, S. Pandya, L.R. Dedon, R.V.K. Mangalam, G.A. Velarde, S. Jesse, N. Balke, A.M. Minor, S.V. Kalinin, L.W. Martin, Nat. Mater. 15 (2016) 549–556.
[9] W. Chun, E.L. David, H.K. Mark, Appl. Phys. Lett. 90 (2007) 172903–172913.
[10] Y. Xueyong, X. Xiaobo, Z. Xiaona, W. Zheng, Y. Mao, D. Jun, W. Di, X. Qingyu, Solid State Commun. 152 (2012) 241–243.
[11] Y. Shihui, L. Lingxia, Z. Weifeng, S. Zheng, D. Helei, Sci. Rep. 5 (2015) 10173.
[12] L. Wei, Z. Qigang, H. Jisong, B. Wangfeng, Z. Jiwei, Integr. Ferroelectr. 140 (2012) 116–122.
[13] C.H. Ming, M.S. Yu, C.L. Ing, H.H. Min, J. Electrochem. Soc. 153 (2006) F260–F265.
[14] S.Z. Yuan, X.J. Meng, J.L. Sun, Y.F. Cui, J.L. Wang, L. Tian, J.H. Chu, Mater. Lett. 65 (2011) 1989–1991.
[15] H.J. Song, T. Ding, X.L. Zhong, J.B. Wang, B. Li, Y. Zhang, C.B. Tan, Y.C. Zhou, RSC Adv. 4 (2014) 60497–60501.
[16] L. Eric, G. Roger, M. Laura, M.B. Lourdes, M. Luis, M.R. Ibarra, H.M. Javier, B. Javier, M. Cesar, A. Pedro, A.P. José, ACS Appl. Mater. Interfaces 7 (2015) 23967–23977.
[17] T. Zhenhua, X. Ying, T. Minghua, X. Yongguang, Z. Wei, Y. Meiling, O. Jun, Z. Yichun, J. Mater. Chem. C 2 (2014) 1427–1435.
[18] D. Denning, J. Guyonnet, B.J. Rodriguez, Int. Mater. Rev. 61 (2016) 46–70.
[19] B. Nina, M. Petro, J. Stephen, H. Andreas, T. Alexander, B.E. Chang, I.K. Ivan, Y. Pu, V.K. Sergei, ACS Nano 9 (2015) 6484–6492.
[20] D.V. Karpinsky, R.C. Pullar, Y.K. Fetisov, K.E. Kamentsev, A.L. Kholkin, J. Appl. Phys. 108 (2010) 042012–042015.
[21] H. Yafei, L. Weili, Z. Tiandong, C. WenPing, Y. Yang, B. Tergul, F. Weidong, J. Phys. Chem. C 120 (2016) 6246–6251.
[22] F. Bi, L. Ruie, L. Miao, G. Kun, T. Yigang, Z. Xuan, G. Baolin, Y. Yaodong, W. Yaping, Mater. Lett. 157 (2015) 311–314.
[23] X. Jingzhong, in: A. Méndez-Vilas (Ed.), Current Microscopy Contributions to Advances in Science and Technology, 2012.
[24] M.T. Escote, F.M. Pontes, E.R. Leite, J.A. Varela, R.F. Jardim, R. Longo, Thin Solid Films 445 (2003) 54–58.
[25] F.M. Pontes, D.S.L. Pontes, E.R. Leite, E. Longo, E.M.S. Santos, S. Mergulhão, A.J. Chiquito, P.S. Pizani, F. Lanciotti Jr, T.M. Boschi, J.A. Varela, J. Appl. Phys. 91 (2002) 6650–6655.
[26] M. Kumaraswamy, R. Ranjith, Mater. Lett. 178 (2016) 23–26.
[27] B. Alexandre, S. ZhenMian, F. Anthony, R. Pascal, D. Rachel, S. Sebastien, RSC Adv. 6 (2016) 32994–33002.
[28] J. Pérez de la Cruz, E. Joanni, P.M. Vilarinho, A.L. Kholkin, J. Appl. Phys. 108 (2010) 114106–114108.
[29] E.B. Araujo, E.C. Lima, I.K. Bdikin, A.L. Kholkin, J. Appl. Phys. 113 (2013) 187206–187208.